Sensors and Actuators A 244 (2016) 324–333

Contents lists available at ScienceDirect

Sensors and Actuators A: Physical

journal homepage: www.elsevier.com/locate/sna

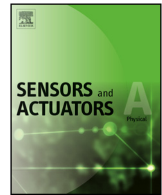

A new design and a fabrication approach to realize a high performance three axes capacitive MEMS accelerometer☆

Akin Aydemir[a,*], Yunus Terzioglu[a,b], Tayfun Akin[a,b]

[a] METU-MEMS Research and Applications Center, Middle East Technical University, Ankara, Turkey
[b] Electrical and Electronics Engineering Department, Middle East Technical University, Ankara, Turkey

ARTICLE INFO

Article history:
Received 29 November 2015
Received in revised form 18 March 2016
Accepted 4 April 2016
Available online 5 April 2016

Keywords:
Three-axis accelerometer
Out of plane accelerometer
Capacitive MEMS accelerometer
SOI

ABSTRACT

This paper presents a new fabrication approach and design for a three axis capacitive MEMS accelerometer that is capable of measuring externally applied accelerations in three orthogonal axes. Individual lateral and vertical axis accelerometers are fabricated in the same die on an SOI wafer which is anodically bonded to a glass substrate. Handle layer of the SOI wafer is used as the top electrode for the vertical axis accelerometer. This accelerometer has a 2 mm^2 perforated electrode area anchored to the glass substrate by four beams. The lateral axis accelerometers on the other hand, have comb finger structures with a 2.7×4.2 mm device size and anchored to the glass substrate by six folded beams. Rest capacitance of the vertical axis accelerometer is designed to be 8.8 pF, and it is 10.2 pF for the lateral axis accelerometers. The system level performance results are obtained using analog readout circuitry integrated to each axis separately. The x- and y-axis accelerometers show a noise floor and bias instability equal or better than 13.9 $\mu g/\sqrt{Hz}$ and 17 μg, respectively, while the z-axis accelerometer shows 17.8 $\mu g/\sqrt{Hz}$ noise floor and 36 μg bias instability values.

© 2016 Elsevier B.V. All rights reserved.

1. Introduction

Micro-Electro-Mechanical Systems and micromachining technologies have enabled the use of miniaturized transducers, actuators, resonators, etc. in many high technology sensor systems due to their small-size, low-cost, and high-reliability compared to the conventional electromechanical systems. This technology has a wide range of application areas including consumer electronics, automotive, and military electronics.

One of the most widely used transducers are the accelerometers, and they have been widely used in inertial navigation, guidance, automobile air bag deployment, and motion control systems. Capacitive MEMS accelerometers have the advantages of having low temperature coefficients, low power dissipation, low fabrication costs, and feasibility of MEMS and IC integration [1]. Due to those advantages, capacitive sensing based MEMS accelerometers have been widely used and received high attention in the MEMS market.

To date, many capacitive accelerometers have been realized using different micro-fabrication technologies, such as surface micromachining [2], bulk micromachining [3], and post CMOS processes [4,5]. Specifically, differential capacitive sensing is a promising approach due to the further advantages including high sensitivity, low noise, and low power dissipation characteristics [1].

In most of the applications mentioned above, three-axis acceleration sensing is desired, and therefore, there is an intensive study in the literature to fabricate high performance three-axis MEMS accelerometers. In these studies, different design concepts and various fabrication approaches are taken into consideration for the implementation. Furthermore, many different approaches have also been reported for the fabrication of individual vertical axis accelerometers [6,7]. These approaches are also used to fabricate monolithic three-axis accelerometers [8,9].

In the early days of MEMS accelerometers, capacitive vertical-axis designs employed varying overlap capacitances. In these accelerometers, the capacitance is measured between movable and stationary vertical comb electrodes. The torsional movement of the suspended electrodes due to an external acceleration results in a change in the overlap area between the electrodes and thus, the applied acceleration can be sensed in terms of capacitance change. However, the accelerometers based on the varying overlap area have low sensitivity compared to the ones based on the varying gap capacitances [10].

☆ Selected paper from EUROSENSORS 2015 conference, September 6-9, 2015, Freiburg, Germany.

* Corresponding author.
E-mail addresses: akina@metu.edu.tr (A. Aydemir), yterzioglu@mems.metu.edu.tr (Y. Terzioglu), tayfuna@metu.edu.tr (T. Akin).

http://dx.doi.org/10.1016/j.sna.2016.04.007
0924-4247/© 2016 Elsevier B.V. All rights reserved.

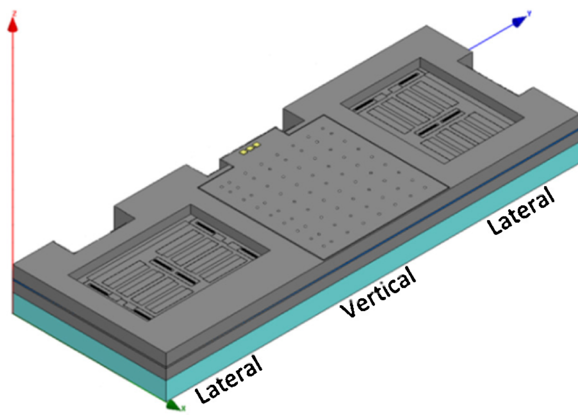

Fig. 1. Schematic drawing of the designed three-axis accelerometer.

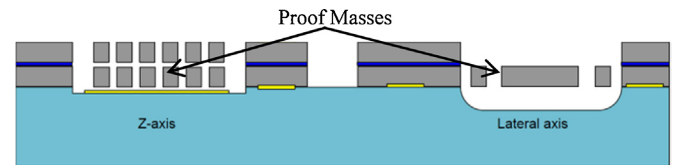

Fig. 2. The cross sectional layout of the designed three-axis accelerometer structure.

Table 1
The specifications of the SOI wafer used in the fabrication process.

Crystal orientation	<100>
Device layer thickness (μm)	35
Buried-oxide thickness (μm)	2
Handle layer thickness (μm)	300
Device layer resistivity (ohm-cm)	0.001–0.004
Handle layer resistivity (ohm-cm)	0.001–0.004

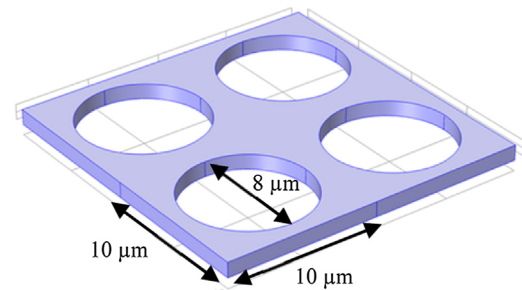

Fig. 3. Proof mass and top electrode structure of the vertical axis accelerometer which is composed of $10 \times 10\,\mu m^2$ unit cells with a 4 μm damping hole radius.

Many vertical-axis capacitive accelerometers are developed using silicon on insulator (SOI) wafers. In those accelerometers, either only one fixed electrode (bottom electrode) under the proof mass [11,12]; or special off-set comb finger structures are used for sensing [13]. However, having only one electrode is not enough for differential sensing, which offers superior linearity performances; and fabrication of off-set comb finger structures requires additional process complexities. Those fabrication approaches have also been used to fabricate single proof mass three axis accelerometers [14,15]. Although extremely small size devices can be fabricated with a single proof mass structure, they suffer from cross-axis sensitivity, limiting their use in high performance applications.

Another approach for achieving three axis acceleration sensing is by assembling two or three single axis accelerometers having similar performances on different substrates. However, this approach increases the packaging size, costs and also causes high cross-axis sensitivities due to highly possible alignment errors during assembly [16].

All of the approaches mentioned above either suffer from non-differential sensing on the vertical axis accelerometer or complicated fabrication processes. Furthermore, it is also important to adapt the fabrication process of the vertical axis accelerometers to the fabrication of lateral ones to achieve a three axis accelerometer on the same substrate.

In this paper, in order to eliminate the deficiencies in the mentioned fabrication and design approaches, first a varying gap differential capacitive vertical axis accelerometer structure is designed where the proof mass of the vertical axis accelerometer is sandwiched between two stationary electrodes defined on the glass substrate and the handle layer of the SOI wafer. Then, the fabrication of this structure is combined with the fabrication of comb finger type lateral axis accelerometers to achieve a three axis accelerometer. Using this approach, individual lateral and vertical axis accelerometers are fabricated on the same die, and thus cross-axis sensitivities due to misalignment are kept as low as possible [17–19]. This paper also presents sensor and system-level test results of each fabricated accelerometer. System-level tests are performed by connecting the accelerometers to an analog readout circuit.

2. Design

Figs. 1 and 2 show the three dimensional and the cross sectional drawings of the designed three-axis accelerometer, respectively. Additionally, the specifications of the SOI wafer used in the fabrication process are given in Table 1.

The fabricated accelerometers are constructed by three major layers. The first layer is the glass substrate on which a recess area for the lateral axis accelerometer is defined. All metal connections and the bottom electrode of the vertical axis accelerometer are also defined on that glass substrate except the top electrode metal connection of the vertical axis accelerometer.

The second layer is the structural layer of the SOI wafer having 35 μm layer thickness. The capacitive gap between the bottom electrode and the proof mass for the vertical axis accelerometer is defined on the surface of that layer. Furthermore, all mechanical structures of the vertical and the lateral axis accelerometers including the proof masses and the spring structures are also defined on that layer.

The third layer is the handle layer of the SOI wafer which is used as the top electrode for the vertical axis accelerometer. The Si section of the handle layer which rests over the lateral axis accelerometer is completely etched away in order to reduce the damping. The sacrificial buried SiO_2 layer of the SOI wafer is used to form the second capacitive gap between the top electrode and the proof mass for the vertical axis accelerometer.

The vertical axis accelerometer has a 2000 μm^2 perforated proof mass structure anchored to the glass substrate with four crab leg spring structures. In order to reduce the damping effect, 4 μm radius damping holes are etched over 10 μm^2 unit cells on the proof mass of the vertical axis accelerometer. Perforation is also defined on the top electrode of the vertical axis accelerometer in order to be able to release the device in wet etcher after the fabrication processes are completed. Fig. 3 shows the perforation hole structure used on the vertical axis accelerometer over the defined unit cells. Table 2 shows the design parameters of the vertical and lateral axis accelerometers.

After designing the mechanical structures, accelerometers are modeled with the Comsol Multiphysics software for the verification. With the Comsol analysis, resonance frequencies of the lateral and vertical axis accelerometers were simulated and results are compared with the hand calculations. To simplify the modal analysis, perforation on the proof mass for the vertical axis accelerometer

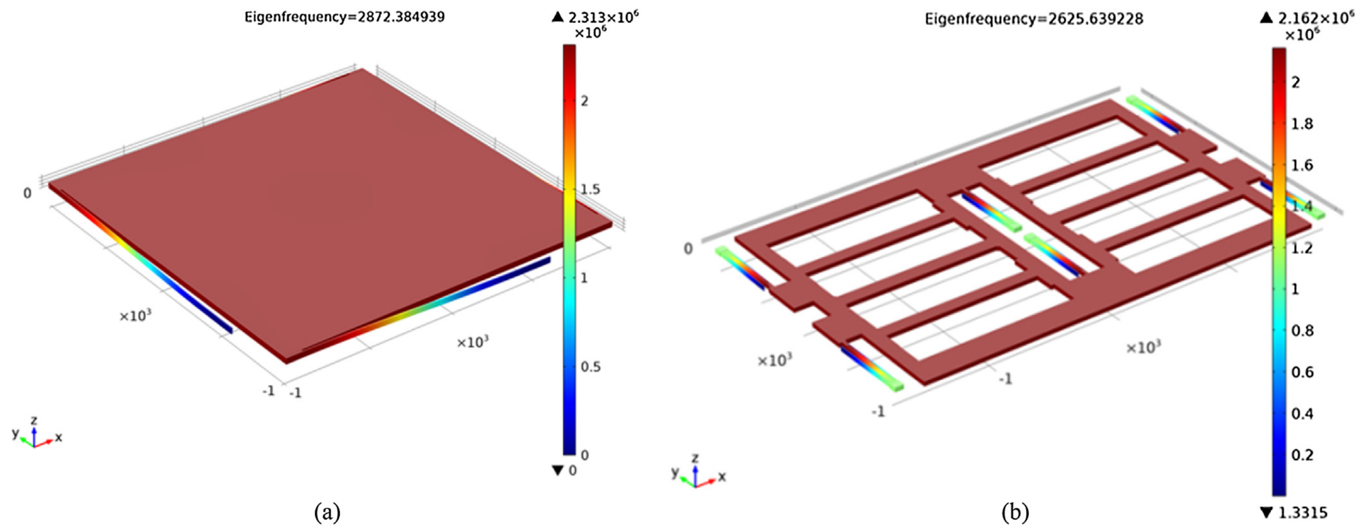

Fig. 4. Mode analysis results for the vertical and lateral axis accelerometers. The resonance frequencies are (a) 2872 Hz for the vertical axis accelerometer (b) 2625 Hz for the lateral axis accelerometer.

Table 2
The design parameters of the vertical and lateral axis accelerometers.

Design Parameters	Vertical	Lateral
Proof mass area (m^2)	2.87×10^{-6}	2.75×10^{-6}
Proof mass (ng)	214	211
Spring constant (N/m)	62.7	56.3
Sensing gap (μm)	2.0	2.0
Resonance frequency (Hz)	2724	2598
Rest capacitance (pF)	8.5	10.5
Brownian noise ($\mu g/\sqrt{Hz}$)	5.9	5.7

Table 3
Simulation results versus hand calculation for the designed lateral and vertical axis accelerometers.

Resonance Frequencies (Hz)	Hand Calculations	Simulation Results
Lateral Axis	2598	2626
Vertical Axis	2724	2872

is excluded from the simulations. In order to compensate for the increase in the inertial mass after such simplification, the density of the Si material is reduced to match the actual mass of the original design. The same approach is also used for the lateral axis accelerometer simulation where the total mass of the fingers is included by adjusting the density of the material.

Table 3 gives the comparison of the simulation results with the hand calculation results, and Fig. 4 shows the deflection of the vertical and lateral axis accelerometers mass in their first mode of operation.

3. Fabrication processes

The fabrication process starts with the glass wafer which is used as the substrate for the lateral and the vertical axis accelerometers.

Glass substrate is patterned with a 0.3 μm thick a-Si layer deposited in a PECVD process. After patterning the masking a-Si layer in SF_6 plasma, the recess area for the lateral axis accelerometer is etched in 49% HF on the glass wafer (Fig. 5a). After stripping the masking material, a-Si layer, Cr/Au layer is deposited to define the contact metallization for the lateral and the vertical axis accelerometers. In that step the bottom electrode of the vertical axis accelerometer is also defined (Fig. 5b).

SOI wafer processes starts with patterning and etching the device layer of the SOI wafer in SF_6 plasma to define the 3 μm capacitive gap between the bottom electrode and the proof mass of the vertical axis accelerometer (Fig. 5c).

In order to define the proof mass of the vertical and the lateral axis accelerometers, the device layer of the SOI wafer is patterned and etched in a DRIE process down to etch stop layer, the buried oxide layer (Fig. 5d).

After cleaning the glass and the SOI wafers in 1:1 piranha solution, wafers are anodically bonded to each other (Fig. 5e).

As a next step, 300 μm thick handle layer of the SOI wafer is thinned to 50 μm thickness in a grinding process (Fig. 5f).

Cr/Au layer is deposited over the thinned handle layer of the SOI wafer and patterned to define the contact metallization for the top electrode of the vertical axis accelerometer (Fig. 5g).

The last DRIE etching is done to define the perforated top electrode of the vertical axis accelerometer on the handle layer of the SOI wafer. The bulk Si layer over the lateral axis accelerometers is also completely etched down to the buried oxide layer in this step (Fig. 5h).

Finally, after the dicing step, devices are released in 1:7 BHF (Fig. 5-i). In order to prevent sticktion, released structures are dried in acetone, IPA, methanol, and hot plate cycle. Since the required undercut level in SiO_2 to release the vertical axis accelerometers is about 3.2 μm, devices are released after about 45 min of 1:7 BHF process.

Fig. 6 shows the SEM images of the fabricated vertical axis and lateral axis accelerometer structures after the releasing and drying steps.

4. Test results

Both sensor- and system-level tests are performed for the verification of the fabricated three axis accelerometers. The change in the capacitances with applied DC bias, the resonance frequencies, and the temperature sensitivities of the electrode capacitances are measured as sensor-level tests. The system-level tests are conducted by integrating the accelerometers with the readout circuit reported in [20] in a hybrid platform three-axis accelerometer package operated at the atmospheric pressure. Noise, non-linearity, and operation range of the accelerometers are measured in the system-level tests.

(a) Recess area formation over the glass wafer for the lateral axis accelerometers.

(b) Metallization to define the bottom electrode of the vertical axis accelerometer and contact metallization for lateral axis accelerometer.

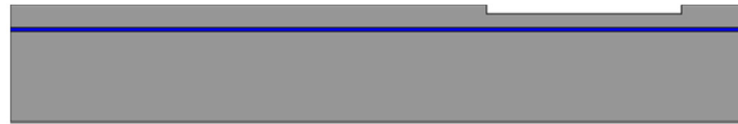

(c) 3 μm gap etching on the SOI wafer for the vertical axis accelerometer.

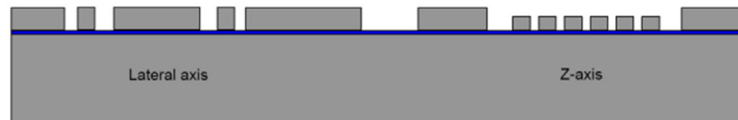

(d) DRIE to define the lateral axis and the vertical axis accelerometer structures.

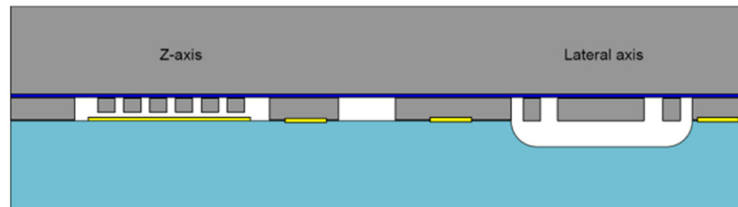

(e) Anodic bonding of the SOI wafer to the glass substrate.

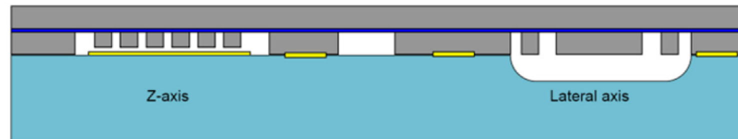

(f) Grinding the handle layer of the SOI wafer to 50 μm thickness.

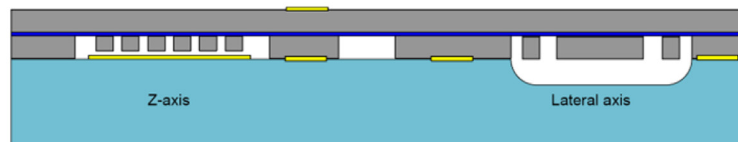

(g) Top electrode metallization for the vertical axis accelerometer.

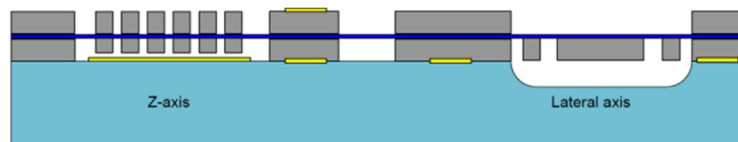

(h) DRIE to define the top electrode of vertical axis accelerometer and to etch the bulk Si over the lateral axis accelerometers.

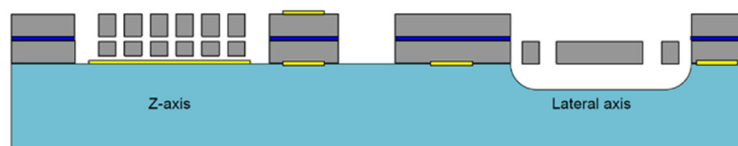

(i) Releasing fabricated accelerometers in 1:7 BHF.

Fig. 5. Three axis accelerometer fabrication process flow.

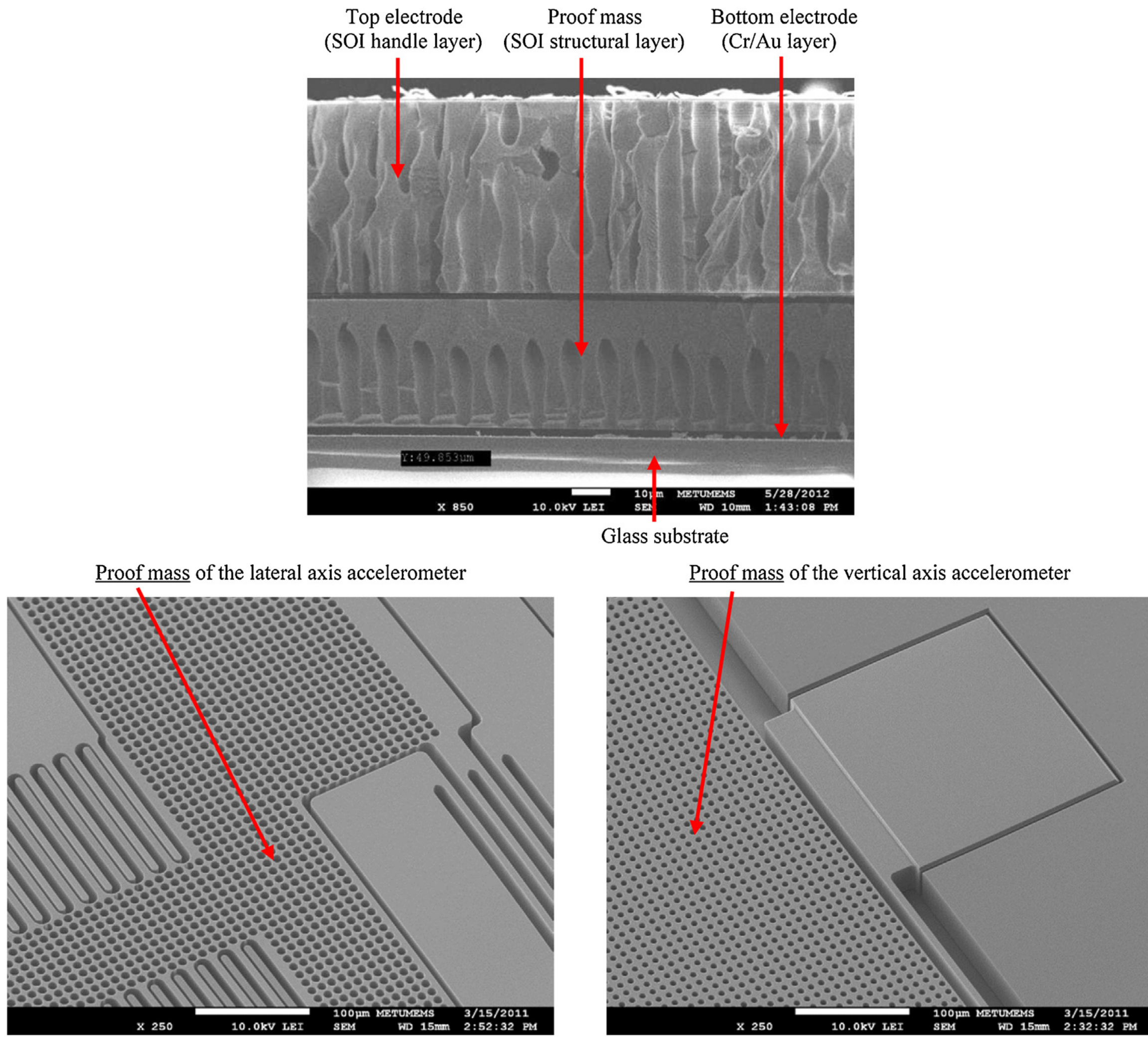

Fig. 6. SEM image of the vertical and lateral axis accelerometers.

Table 4
The sensor connection diagram with respect to path numbers.

Pad #	Lateral	Pad #	Vertical
1 & 7	Fixed electrode 1	4	Top Electrode
3 & 9	Fixed electrode 2	6	Bottom Electrode
2 & 8	Proof mass	5	Proof mass
10	Ground	10	Ground

4.1. Sensor level tests—capacitance-voltage (C-V) change

The capacitance-voltage change tests are performed on the fabricated three axis accelerometer for verifying the functionality of the accelerometers.

The functionality of the lateral and vertical accelerometers on the same die are separately determined by applying a DC bias between the proof mass and one of the stationary electrodes, while the other electrode is connected to ground. Furthermore, bulk Si layer around the accelerometer on the structural and handle layer of the SOI wafer are also grounded during the sensor level tests to prevent the effect of any parasitic capacitances.

Fig. 7 shows the pad diagram of the fabricated accelerometer. The descriptions of the numbered pads shown in Fig. 7 are given in Table 4. Note that pad 10 is the grounding connection for the bulk Si layer around the accelerometer on the structural and handle layer of the SOI wafer.

Table 5
Comparison of hand calculation and measurement results for the rest capacitance, and change in the capacitance with the applied DC bias for the lateral and vertical axis accelerometers. An increase in the rest capacitance and sensitivity is observed due to the fringing field effect exist on the vertical axis accelerometer due to the perforation as observed on the capacitive simulations.

	Accelerometer	C_{Rest} (pF)		C-V (fF) Change at ±2V	
		1st Elec.	2nd Elec.	1st Elec.	2nd Elec.
Designed	Lateral (x)	10.3	10.5	181	181
	Lateral (y)	10.3	10.5	181	181
	Vertical	8.5	8.5	67	67
Measured	Lateral (x)	11.62	11.69	212	220
	Lateral (y)	11.69	11.68	224	205
	Vertical	11.03	11.27	196	208

Fig. 8 shows the C-V measurement results for the lateral and vertical axis accelerometers. The test results and the theoretical calculations are in good agreement with each other for both lateral and vertical axis accelerometers. However, it should be noted that an increase in the rest capacitance for the vertical axis accelerometer has been observed due to the fringing field effect. This increase was also observed during the capacitive simulations of the vertical axis accelerometer.

Table 5 shows the comparison of hand calculation and measurement results for the rest capacitance and the change in the

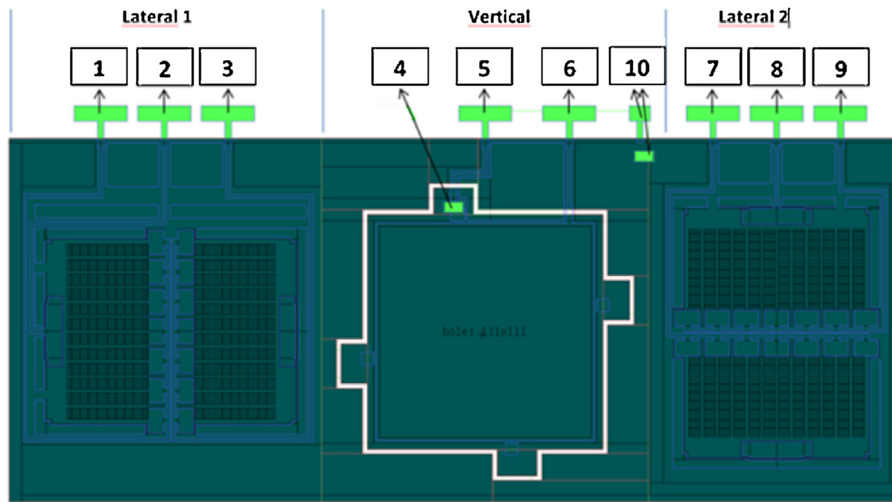

Fig. 7. The pad diagram of the fabricated three axis accelerometer.

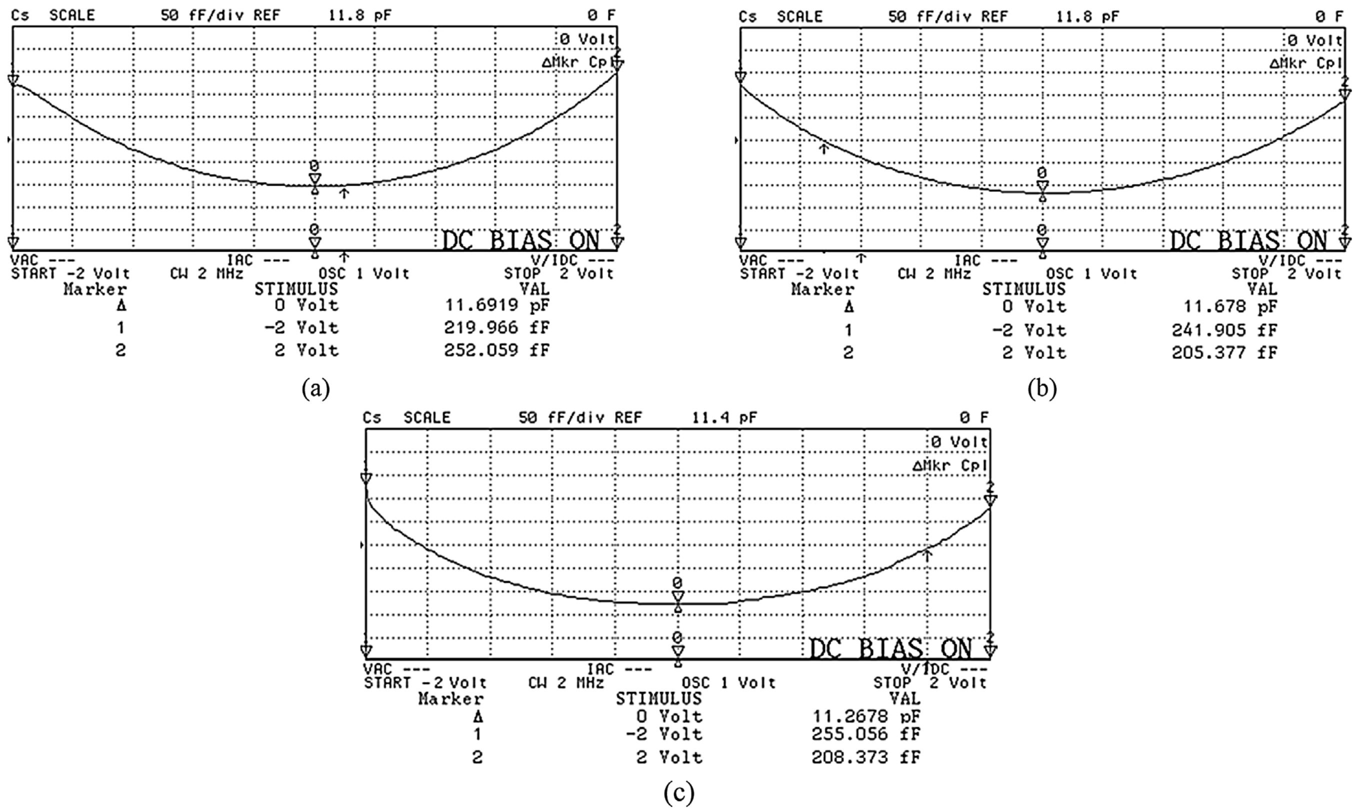

Fig. 8. C-V measurement results for the lateral (a,b) and vertical (c) axis accelerometers, respectively.

capacitance with the applied DC bias for the lateral and vertical accelerometers.

4.2. Sensor level tests—resonance frequency

The resonance frequencies of accelerometers are individually measured to determine the dynamic response of the lateral and vertical accelerometers using a dynamic signal analyzer. During these tests, the accelerometers are actuated with an AC signal at frequencies ranging from 2 kHz to 3 kHz while the proof mass is biased with a DC voltage of 1 V under a controlled vacuum environment. Fig. 9 shows the resonance characteristics of the lateral and vertical accelerometers.

Table 6
Simulation versus measurement results of the resonance frequencies of the three-axis accelerometer.

Resonance Frequencies (Hz)	Simulation Results	Measurement Results
Lateral Accelerometer	2626	2390
Vertical Accelerometer	2872	2683

Table 6 summarizes simulation versus measurement results of the resonance frequencies of the three-axis accelerometer. It should be noted that measurement results are in good agreement with the theoretical calculation results for both lateral and vertical axis accelerometers.

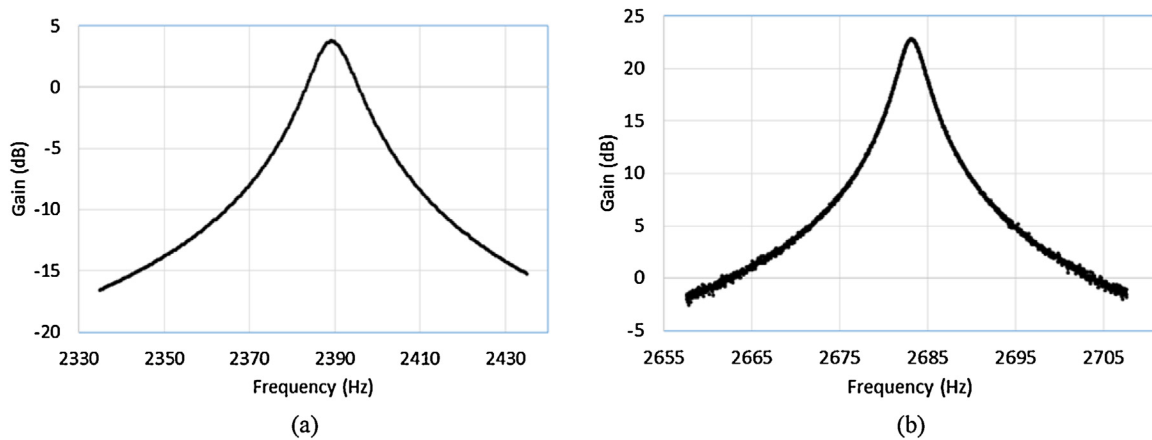

Fig. 9. The resonance frequency measurement results for (a) lateral and (b) vertical accelerometers.

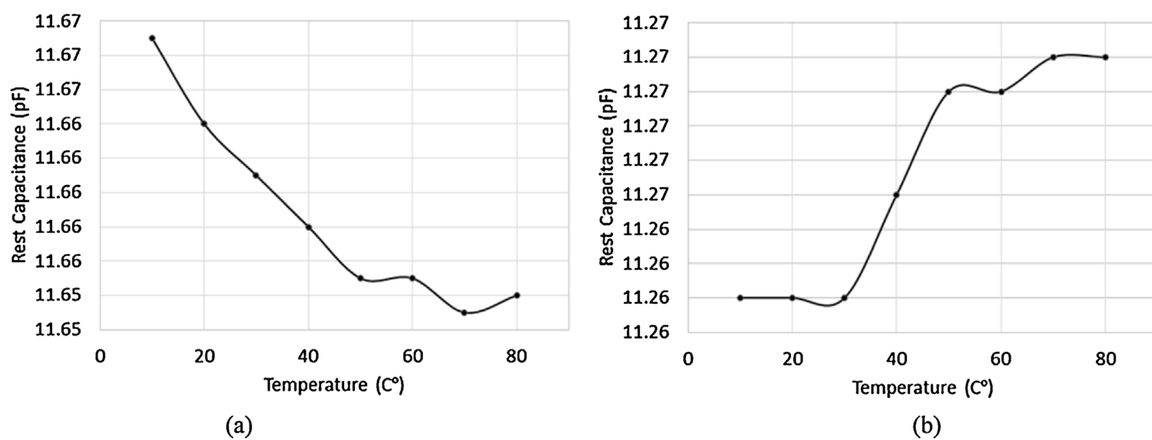

Fig. 10. The rest capacitance measurement results for the (a) lateral and (b) vertical axis accelerometers with the change in the temperature. Change in the capacitance value with the temperature is so small compared to the rest capacitance of the accelerometers that it can be neglected.

4.3. Sensor level tests—temperature tests

The temperature sensitivities of the electrode capacitances are measured in a range from 10 °C and 80 °C using a temperature controlled probe station. Fig. 10 shows the results of these measurements for the lateral and vertical axis accelerometers.

4.4. The system level test results

The fabricated three-axis accelerometer is integrated with the readout circuit reported in [20] to prepare a hybrid platform three-axis accelerometer package operated at the atmospheric pressure. Fig. 11 shows the prepared accelerometer package placed on the test PCB.

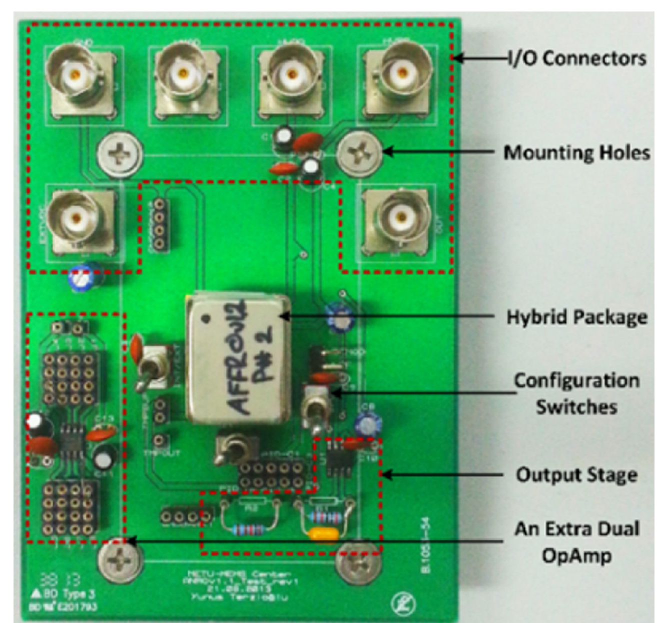

Fig. 11. The prepared hybrid platform accelerometer package on the test PCB.

Fig. 12 shows the Allan Variance test results of lateral and vertical accelerometers. The noise floors of lateral and vertical accelerometers are extracted from the Allan Variance graphs. It is 13.9, 13.2, and 17.8 $\mu g/\sqrt{Hz}$ for x-, y-, and z-axis, respectively. The bias instability values are also extracted from the Allan Variance plots, and they are measured as 17 µg, 16 µg, and 36 µg for lateral (x- and y-axis) and vertical (z-axis) accelerometers, respectively.

Non-linearity of the three-axis accelerometer is measured by using a centrifuge table. The non-linearity data are evaluated with respect to a best-fit line. Fig. 13 shows the normalized non-linearity test results of the three-axis accelerometer. Additionally in Fig. 14, the deviation of the accelerometer response from an ideal line-fit is given. Based on this test, the non-linearity performance of the

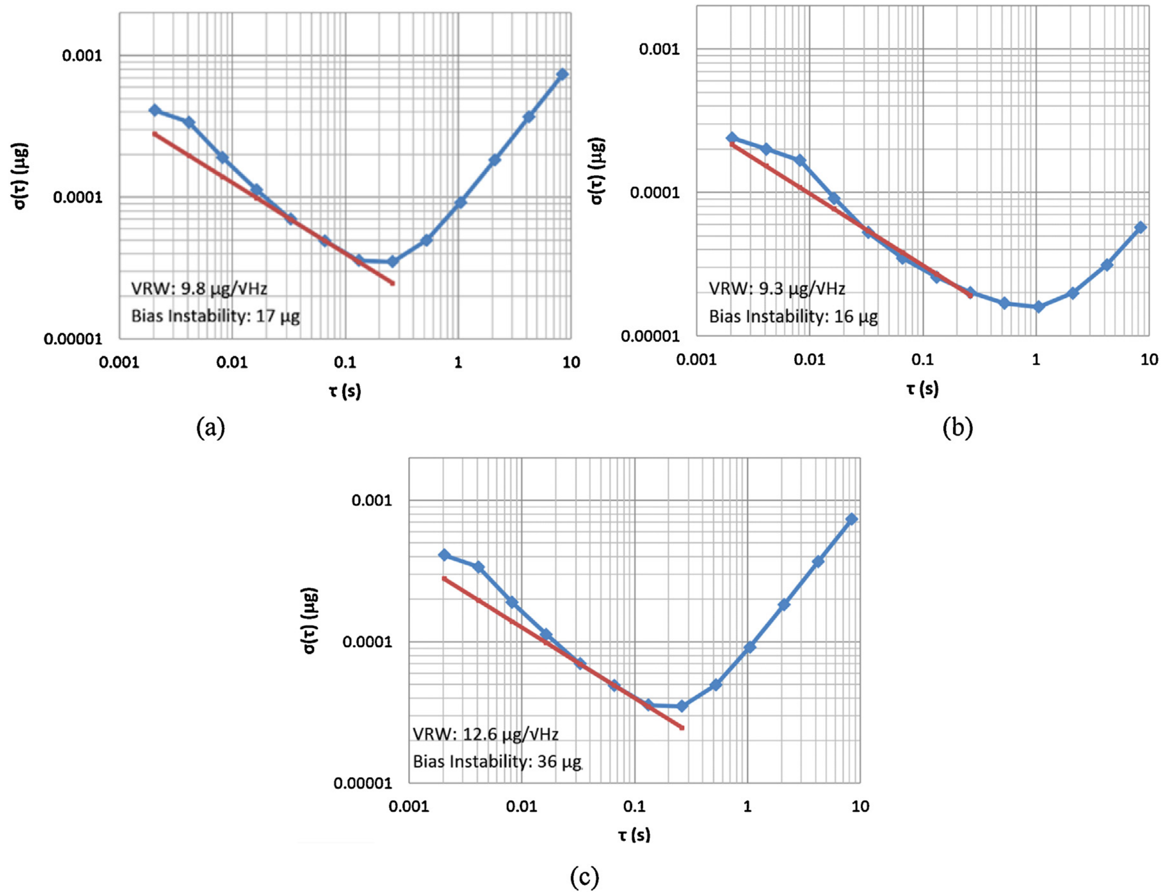

Fig. 12. Allan Variance results showing the velocity random walk (VRW) and the bias instability for (a) x, (b) y, and (c) z-axis accelerometers. Considering the range of the accelerometers, relatively low VRW results are achieved for all individual accelerometers.

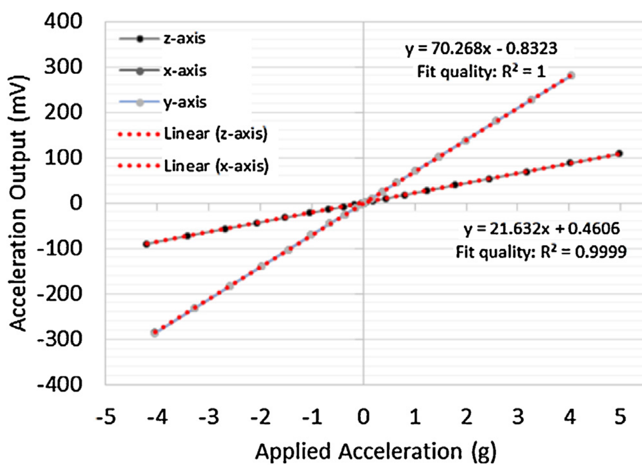

Fig. 13. Linearity test results of the three-axis accelerometer, which shows 0.26%, 0.28%, and 0.30% non-linearity for x-, y-, and z- axis, respectively, where the achieved non-linearity results are very low compared to its counterparts. Note that x- and y-axis results overlap. Also note that the measurement data is normalized at 0 mV in this figure for a better visualization.

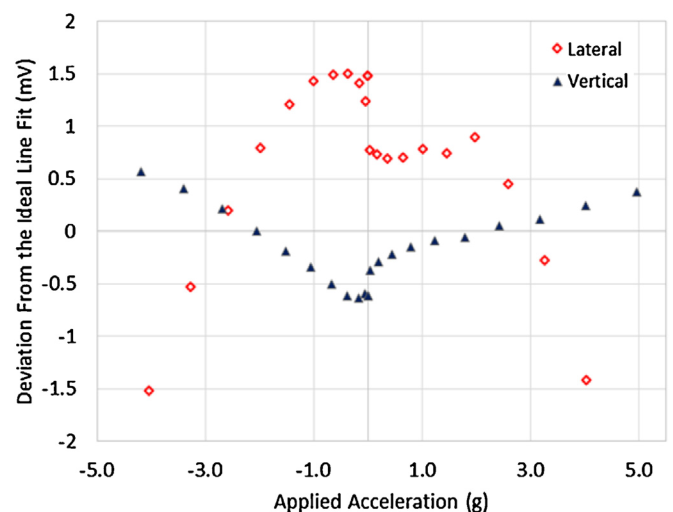

Fig. 14. The deviation of the measured centrifugal test data from the fitted ideal line for lateral and vertical axis accelerometers.

accelerometers are calculated as 0.26%, 0.28%, and 0.30% for x-, y-, and z-axis, respectively for the measurement range of −4 to +4 g.

The cross-axis sensitivity of the fabricated three-axis accelerometer is determined by applying ±1 g by rotating the test system around one axis while the acceleration data have simultaneously been collected for all three axes. Then, the cross-axis sensitivity of the three-axis accelerometer is extracted from the collected data.

Table 7 shows the cross-axis sensitivity results of the three-axis accelerometer. It should be noted that even though the process ensures orthogonal alignment of all three accelerometers, the placement of the sensor inside the hybrid package can still cause erroneous readings without any significant effect on the cross-axis sensitivity performance.

Table 8 summarizes the system-level performance results of the fabricated three-axis accelerometer.

Table 7
Cross-axis sensitivity results of the three-axis accelerometer. Getting better cross-axis sensitivity for the vertical axis accelerometer compared to the lateral ones is due to the electrode design of that accelerometer, where the top and bottom electrode have a slightly larger electrode area compared to the proof mass.

Acceleration Input	Output		
	x	y	Z
X	–	0.92%	0.63%
Y	0.89%	–	0.62%
Z	0.21%	0.36%	–

Table 8
The performance results of the three-axis accelerometer.

	X	y	Z
White Noise ($\mu g/\sqrt{Hz}$)	13.9	13.2	17.8
Bias Instability (μg)	17	16	36
Measured Range (g)	±4	±4	±4
Estimated Range (g)	71	71	231
Non-linearity (%)	0.26	0.28	0.30
Scale Factor (mV/g)	70.27	70.42	21.63
Zero-g Offset (g)	1.2	0.7	−10

Table 9 presents a comparison of the device performance for the current three-axis accelerometer with respect to three-axis accelerometers fabricated for commercial and academic purposes.

5. Conclusion

A three-axis MEMS accelerometer with differential capacitive sensing capability for all three axes has been designed and fabricated successfully using an SOI wafer anodically bonded to a glass substrate. Individual lateral and vertical axis accelerometers are fabricated on a single die to achieve three axis acceleration sensing. The dimensions of the fabricated three axis accelerometer structure are $11.8 \times 4.8 \times 0.6\,mm^3$.

First, a varying gap differential capacitive sensing vertical axis accelerometer structure is designed, where the proof mass of the vertical axis accelerometer is sandwiched between two stationary electrodes defined on the glass substrate and the handle layer of the SOI wafer. Then, the developed fabrication approach for this structure is combined with the fabrication of comb finger type lateral axis accelerometers to achieve a three axis accelerometer on a single substrate.

Both sensor- and system-level tests are performed on the fabricated three axis accelerometer for the verification of the accelerometers.

The measured noise floor and bias instabilities are equal or better than $14\,\mu g/\sqrt{Hz}$ and $17\,\mu g$ for the x- and y- axis accelerometers, respectively, while the results for the z-axis accelerometer are $17.8\,\mu g/\sqrt{Hz}$ noise floor and $36.0\,\mu g$ bias instability. These noise performances are achieved with a measurement range of over ±4 g for the x-, y-axis, and z-axis accelerometers with non-linearity values equal to or less than 0.3%.

References

[1] D.K. Shaeffer, MEMS inertial sensors: a tutorial overview, IEEE Commun. Mag. 51 (no. 4) (2013) 100–109.
[2] B.E. Boser, R.T. Howe, Surface micromachined accelerometers, IEEE J. Solid State Circuits 31 (3) (1996) 366–375.
[3] K. Kwon, S. Park, A bulk-micromachined three-axis accelerometer using silicon direct bonding technology and polysilicon layer, Sens. Actuators A 66 (1998) 250–255.
[4] H. Luo, G. Zhang, L.R. Carley, G.K. Fedder, A post-cMOS micromachined lateral accelerometer, J. Microelectromech. Syst. 11 (3) (2002) 188–195.
[5] C.-M. Sun, M.-H. Tsai, Y.-C. Liu, W. Fang, Implementation of a monolithic single proof-mass tri-axis accelerometer using CMOS-mEMS technique, IEEE Trans. Electron. Devices 57 (7) (2010) 1670–1679.
[6] C. Wang, M.H. Tsai, C.M. Sun, W. Fang, A novel CMOS out-of-plane accelerometer with fully differential gap-closing capacitance sensing electrodes, J. Micromech. Microeng. 17 (2007) 1275–1280.
[7] C.P. Hsu, M.C. Yip, W. Fang, 'Implementation of a gap-closing differential capacitive sensing Z-axis accelerometer on an SOI wafer, J. Micromech. Microeng. 19 (2009) 1–7, 075006.
[8] J. Chae, H. Kulah, K. Najafi, A monolithic three-axis micro-g micromachined silicon capacitive accelerometer, IEEE J. Microelectromech. Syst. 14 (2005) 235–242.
[9] M. Lemkin, N. Ortiz, B.E. Boser, J.H. Smi, A 3-axis surface micromachined ΣΔ accelerometer, 44th ISSCC vol. 457 (1997) 202–203.
[10] A. Selvakumar, F. Ayazi, K. Najafi, A high sensitivity Z-axis capacitive silicon microaccelerometer with a torsional suspension, J. Microelectromech. Syst. 7 (2) (1998).
[11] O. Sidek, M. Afif, M.A. Miskam, Design and simulation of SOI-mEMS Z-axis capacitive accelerometer, Int. J. Eng. Technol. IJET-IJENS 10 (06) (2010).
[12] Y. Matsumoto, M. Nishimura, M. Matsuura, M. Ishida, Three-axis SOI capacitive accelerometer with PLL C–V converter, Sens. Actuators 75 (1999) 77–85.
[13] H. Hamaguchi, K. Sugano, T. Tsuchiya, O. Tabata, A differential capacitive three-axis SOI accelerometer using vertical comb electrodes, Solid-State Sens. Actuators Microsyst. Conf. (2007).
[14] M.A. Lemkin, B.E. Boser, D. Auslander, J.H. Smith, A 3-axis force balanced accelerometer using a single proof-mass, in: Proc. Transducers, Chicago, IL, USA, June, 1997, pp. 1185–1188.
[15] S.-C. Lo, C.-K. Chan, W.-C. Lai, M. Wu, Y.-C. Lin, W. Fang, Design and implementation of a novel poly-si single proof-mass differential capacitive-sensing 3-axis accelerometer, in: Proc. Transducers Eurosensors, Barcelona, Spain, June, 2013, pp. 1819–1822.
[16] N.F. Watson, Accelerometer system, U.S. Patent 4 601 206 A, July. 22, (1986).
[17] A. Aydemir, A Three Axis Capacitive MEMS Accelerometer on a Single Substrate, Ph.D. Dissertation, Middle East Technical University, Turkey, 2013.
[18] A. Aydemir, T. Akin, A Three Axis Capacitive MEMS Accelerometer on a Single Substrate, PCT/TR2014/000531, December, (2014).
[19] A. Aydemir, T. Akin, Process development for the fabrication of a three axes capacitive MEMS accelerometer, Procedia Eng. 120 (2015) 727–730.
[20] Y. Terzioglu, K. Azgin, T. Akin, A simple out-of-plane capacitive MEMS accelerometer utilizing lateral and vertical electrodes for differential sensing, in: IEEE Sensors Conference, Busan, South Korea, November, 2015.
[21] ADXL377-Small, Low Power, 3-Axis ±200 g Accelerometer, Analog Devices, Norwood, MA, USA, (2012).

Table 9
The comparison of performance results of the three-axis accelerometers in literature. Designed three axis accelerometer in this study provides a low noise with a reasonable range, as well as low cross axis sensitivity and low non-linearity compared to its counterparts presented in Table below.

References	Noise ($\mu g/\sqrt{Hz}$)			Range (g)	Cross-Axis	Non-linearity
	x	y	z			
[5]	120,000	271,000	357,000	Meas. Range ±0.8–6	<8.3%	2.6%, 3.2%, and 3.4%
[8]	1.6	1.6	1.1	±1	–	–
[14]	730	730	760	11 for lateral, 5.5 for vertical	–	–
[15]	–	–	–	Meas. Range 0.1–3	6.8%, 6.8% and 9.0%	2.7%, 2.6%, and 2.9%
[21]	2700	2700	4300	±200	±1.4%	±0.5%
[22]	400	200	900	Meas. Range 0.01–2	3%, 2.3% and 8.8%	1%, 0.5% and 2.4%
[23]	12	14	110	3.2 for lateral, 5.1 for vertical	<4.73%	
[24]	5.4	5.5	12.6	±10 for lateral +12/−7.5 for vertical	<1%	0.34%, 0.28%, and 0.41%
This Study	13.9	13.2	17.8	Measured ±4 for lateral and vertical Estimated ±71 for lateral and ±231 vertical	<1%	0.26%, 0.28%, and 0.30%

[22] Y.-C. Liu, M.-H. Tsai, S.-S. Li, W. Fang, A fully-differential, multiplex-sensing interface circuit monolithically integrated with triaxis pure oxide capacitive CMOS-mEMS accelerometers, in: Proc. Transducers Eurosensors XXVII, Spain, 2013, pp. 610–613.
[23] H. Qu, D. Fang, H. Xie, A monolithic CMOS-mEMS 3-axis accelerometer with a low-noise, low-power dual-chopper amplifier, EEE Sens. J. 8 (September (9)) (2008) 1511–1518.
[24] S. Tez, U. Aykutlu, M.M. Torunbalci, T. Akin, A bulk-micromachined three-axis capacitive MEMS accelerometer on a single die, J. Microelectromech. Syst. 24 (5) (2015).

Biographies

Akin Aydemir was born in Osmaniye, Adana, Turkey, in 1980. He received the B.S. and M.Sc degrees from Department of Physics, Middle East Technical University (METU), Ankara, in 2004, and 2007, respectively and Ph.D. degree from the Department of Micro and Nanotechnology, METU, Ankara, in 2013. He has been working as a Research and Process Development Engineer at the METU-MEMS Research and Applications Center since 2004. His major research interests include the design, simulation, and fabrication of microelectromechanical systems inertial sensors and micro bolometers.

Yunus Terzioglu was born in Antalya, Turkey in 1989. He received the B.S. and M.Sc degrees from electrical engineering, METU, Ankara, in 2012 and 2015, respectively. He currently is a Ph.D. student at electrical engineering, METU, Ankara, Turkey, and has been working as a research engineer at METU – MEMS Research and Applications Center since 2012.

Tayfun Akin was born in Van, Turkey, in 1966. He received the B.S. degree in electrical engineering from METU, Ankara, in 1987, and the M.S. and Ph.D. degrees in electrical engineering from the University of Michigan, Ann Arbor, in 1989 and 1994, respectively. He went to the USA in 1987 for his graduate studies with a graduate fellowship provided by the NATO Science Scholarship Program through the Scientific and Technical Research Council of Turkey. Since 1995, 1998, and 2004, he has been an Assistant Professor, an Associate Professor, and a Professor, respectively, with the Department of Electrical and Electronics Engineering, METU. He is the Director of the METU-Microelectromechanical Systems (MEMS) Center.